Mapping the binocular scotoma in macular degeneration

Cécile Vullings Smith-Kettlewell Eye Research Institute, San Francisco, CA, USA

Preeti Verghese Smith-Kettlewell Eye Research Institute, San Francisco, CA, USA

When the scotoma is binocular in macular degeneration (MD), it often obscures objects of interest, causing individuals to miss information. To map the binocular scotoma as precisely as current methods that map the monocular scotoma, we propose an iterative eye-tracker method. Study participants included nine individuals with MD and four age-matched controls. We measured the extent of the monocular scotomata using a scanning laser ophthalmoscope/optical coherence tomography (SLO/OCT). Then, we precisely mapped monocular and binocular scotomata with an eye tracker, while fixation was monitored. Participants responded whenever they detected briefly flashed dots, which were first presented on a coarse grid, and then at manually selected points to refine the shape and edges of the scotoma. Monocular scotomata measured in the SLO and eye tracker are highly similar, validating the eye-tracking method for scotoma mapping. Moreover, all participants used clustered fixation loci corresponding to their dominant preferred fixation locus. Critically, for individuals with binocular scotomata, the binocular map from the eye tracker was consistent with the overlap of the monocular scotoma profiles from the SLO. Thus, eye-tracker-based perimetry offers a reliable and sensitive tool for measuring both monocular and binocular scotomata, unlike the SLO/OCT that is limited to monocular viewing.

Introduction

Macular degeneration (MD) affects the central part of the retina at and around the fovea, resulting in a scotoma. When MD is present in both eyes, it can create a binocular scotoma that obscures objects in the central visual field and lead to the development of a new locus for fixation (e.g. Timberlake, Mainster, Webb, Hughes, & Trempe, 1982; Von Noorden & Mackensen, 1962). Individuals are often not aware of the location of their binocular scotoma, which can create difficulties in tasks of daily living (Fletcher, Schuchard, & Renninger, 2012; Safran & Landis, 1999). This lack of awareness has been attributed to the phenomenon of filling-in, where cortical processes perceptually complete missing information by extrapolating the background (Zur & Ullman, 2003), although this challenge has not been addressed under binocular viewing and it is unclear how the nature of the stimulus affects this phenomenon (Cohen, Lamarque, Saucet, Provent, Langram, & LeGargasson, 2003).

The binocular scotoma results from an overlap of the two monocular scotomata and determines functional vision in the real world. The residual vision outside the scotoma along with factors, such as where it is placed with respect to the eccentric fixation locus, determines performance in tasks including eye-hand coordination (e.g. Verghese, Tyson, Ghahghaei, & Fletcher, 2016), navigation (e.g. Aspinall, Borooah, Alouch, Roe, Laude, Gupta, Gupta, Montarzino, & Dhillon, 2014), facial recognition (e.g. Bernard & Chung, 2016), visual search (e.g. Van der Stigchel, Bethlehem, Klein, Berendschot, Nijboer, & Dumoulin, 2013), and reading (see Chung, 2020 for a review). Therefore, directly measuring the location and extent of the binocular scotoma is crucial for evaluating residual functional vision when observers naturally interact with the world. Importantly, a direct measure of the binocular scotoma addresses two critical concerns with using monocular measurements to predict binocular function.

The binocular scotoma can be estimated from monocular maps if the alignment of the two eyes is known. Although studies have reported that under binocular viewing, gaze in the worse eye is often aligned with the gaze of the fixation locus in the better eye (Kabanarou, Crossland, Bellmann, Rees, Culham, & Rubin, 2006; Tarita-Nistor, Eizenman, Landon-Brace, Markowitz, Steinbach, & González, 2015), we make no assumptions about the alignment of gaze. Additionally, binocular rivalry suppression often occurs during monocular viewing, particularly when the dominant eye is covered (Ellingham, Waldock, & Harrad, 1993), and can transiently lead to loss of vision and impact the estimation of a monocular scotoma map. By directly measuring the functional scotoma under binocular viewing conditions, we

Citation: Vullings, C., & Verghese, P. (2021). Mapping the binocular scotoma in macular degeneration. *Journal of Vision*, *21*(3):9, 1–12, https://doi.org/10.1167/jov.21.3.9.

https://doi.org/10.1167/jov.21.3.9 Received November 20, 2020; published March 5, 2021 ISSN 1534-7362

avoid potential confounds of monocular viewing and the possibility of misalignment between the eyes.

Presently, monocular visual field-testing methods, such as automated perimetry in the Humphrey Field Analyzer, can determine the coarse boundary of a monocular scotoma. Finer spatial detail of the monocular scotoma can be obtained with manual selection of points for microperimetry in the scanning laser ophthalmoscope (SLO) or other methods, such as patient-tailored fundus-controlled perimetry (Pfau, Müller, Von der Emde, Lindner, Möller, Fleckenstein, Holz, & Schmitz-Valckenberg, 2020). Spectral-domain optical coherence tomography (OCT) methods that determine the thickness of specific retinal layers can also reliably identify visual field defects (e.g. Acton, Smith, Hood, & Greenstein, 2012; Brandao, Ledolter, Schötzau, & Palmowski-Worlfe, 2016; Nilforushan, Nassiri, Moghimi, Law, Giaconi, Coleman, Caprioli, & Nouri-Mahdavi, 2012; Urata, Mariottoni, Jammal, Ogata, Thompson, Berchuck, Estrela, & Medeiros, 2020). Although these methods can map the region of the retinal lesion in detail, none of them can directly determine the binocular field defect (but see Chung, Li, Ağaoğlu, Tiruveedhula, & Roorda, 2020, who used a custom-built binocular SLO with a maximum aperture of 10 degrees). The binocular scotoma can be estimated approximately by the California Central Visual Field test (Mattingly Low Vision Inc., Escondido, CA, USA), which maps the binocular scotoma in response to laser points flashed on a circular grid, while the patient fixates the center, although fixation is not monitored. Other studies have suggested different ways to map the binocular scotoma with an eye tracker (e.g. Janssen & Verghese, 2016; Shanidze & Verghese, 2019; Sullivan & Walker, 2015; Van der Stigchel et al., 2013; Wiecek, Jackson, & Bex, 2015) but the spacing of probed regions was predetermined and not well-tailored to map individual scotoma profiles.

In this study, we propose a novel eye-tracker-based method to map the absolute binocular scotoma with precision and flexibility in a wide visual field, while carefully monitoring gaze position. The critical feature of this method is the adaptive nature of the mapping procedure based on previous measurements. We show that monocular measurements in the eye tracker are highly similar to monocular microperimetry in the SLO using a manual selection of test locations. Furthermore, binocular measurements in the eye tracker provide a direct estimate of the functional binocular scotoma, without any need for estimating this scotoma from monocular measurements and the attendant concerns of gaze alignment and binocular rivalry suppression.

Materials and methods

Participants

Nine adults with MD (56–89 years old, 3 women) and four age-matched controls (58–74 years old, 3 women) participated in this research. Control participants (C) had normal or corrected-to-normal vision. Seven participants with MD had age-related MD in one or both eyes and two had Stargardt's disease. Three participants had nonoverlapping monocular scotomata (M) and six had a binocular scotoma (B). All participants with a binocular scotoma were referred to us by the low-vision rehabilitation practice of Dr. Donald Fletcher at the Pacific Vision Foundation. All experimental procedures were approved by the Institutional Review Board of the Smith-Kettlewell Eye Research Institute and followed the tenets of the Declaration of Helsinki. All participants gave informed written consent after an explanation of the nature and possible consequences of the study, and received monetary compensation for their participation.

Apparatus

Stimuli were generated using Psychophysics Toolbox (Brainard, 1997; Pelli, 1997) for MATLAB (MathWorks, Natick, MA, USA) and displayed on a large projection screen (40.36 × 30.27 degrees), illuminated from behind by a Mitsubishi XD490U DLP projector. Participants were seated on a height-adjustable chair in a darkened room facing the center of the screen at a viewing distance of 1 m, with their heads in a chin and forehead rest, to minimize measurement errors. When viewing was binocular, only the position of the better/dominant eye was monitored in the eye tracker. When viewing was monocular, the viewing eye was tracked and the other eye was occluded. Eye movements were measured continuously with an infrared video-based eye tracking system (Eyelink, SR Research Ltd., Ontario, Canada), sampled at 1000 Hz. Data were transferred, stored, and analyzed via programs written in MATLAB running on a Windows computer.

The fixation cross (1 degree) and probe dots (diameter 0.5 degrees), both with luminance of 283.6 cd/m^2 were displayed on a background of luminance 78.85 cd/m^2. The Weber contrast of the cross and dots was 2.5967.

Before each experimental session, we calibrated the eye tracker by having the subject fixate with their fovea or preferred retinal locus (PRL) a set of five fixed locations at the center and the ends of a cross of 10 degrees extent, as we wanted to monitor fixation

ID	Sex	Age	Binocular acuity (logMAR)	Monocular acuity OS (logMAR)	Monocular acuity OD (logMAR)	Dominant eye PRL eccentricity (deg)	Fellow eye PRL eccentricity (deg)
Patients							
B1	M	77	1.18	1.2	1.18	[−8.8 to −23.2]	[−7.1 to −25.9]
B2	F	76	0.3	0.81	0.4	[−0.7 to −0.8]	[−1.0 to 0.4]
B3	M	57	1.1	1.1	1.2	[−1.9 to −5.5]	[−2.9 to −4.2]
B4	F	87	0.5	1.18	0.52	[−4.5 to −1.5]	[−7.0 to −2.0]
B5	M	89	0.44	Ø	0.46	[−3.2 to −4.42]	[−0.7 to −2.9]
B6	M	59	1.55	Ø	Ø	[6.7 to 26.3]	[−8.2 to 22.3]
M1	M	75	0.1	1.3	0.1		[−2.7 to −6.4]
M2	F	78	0.0	0.59	0.03		[−6.0 to −5.7]
M3	M	79	0.18	0.18	0.18		
Controls							
C1	F	65	0.44	0.62	0.56		
C2	F	74	0.26	0.54	0.26		
C3	M	61	0.6	0.88	0.6		
C4	F	58	0.0	0.3	0.0		

Table 1. Participant characteristics. The PRL eccentricity was obtained by computing the BCEA of eye positions during 10 second fixation stability test in the SLO, using the center of mass of this BCEA and calculating its distance in degrees from the anatomic foveal pit obtained in the OCT (when available, see text). Note: PRL eccentricity is not provided for M3 as this participant did not have a central scotoma, and had foveal sparing. Ø means the visual acuity could not be measured.

stability near the preferred retinal locus. The size of the typical calibration annular target was increased (diameter 1.5 degrees, annulus width 0.7 degrees) to improve visibility for participants with MD. The calibration was accepted only if the mean validation error was below 1 degree. Every 15 trials, we rechecked calibration by having participants look at the calibration target displayed in the center of the screen for a 1-point calibration check.

Procedure

Scotoma mapping in the SLO/OCT

Prior to testing, we measured the monocular and binocular visual acuity for all participants. We also mapped monocular scotomata and the locations of the optic discs in each eye using microperimetry with unattenuated 0-dB dots (dot luminance, 125 cd/m^2; Weber contrast, 12.5) with a scanning laser ophthalmoscope (SLO/OCT; Optos, Marlborough, MA, USA), which probes a field size of 29.7 degrees. A custom arrangement of points was used to determine the scotoma profile. Fixation stability was also measured by using a 10-second fixation target and was characterized by a bivariate contour ellipse area (BCEA) (Steinman, 1965). The PRL was assigned to the center location of the BCEA fit to the fixation data. When possible, the foveal pit location was estimated from OCT to calculate the eccentricity of the PRL in each eye. If we could locate the foveal pit in one eye but not in the other, we assumed that it was at a similar distance from the center of the optic disc. If neither foveal pit could be visualized, the location of the fovea was estimated using normative data of foveal distance (i.e. 15 degrees horizontally and 1.5 degrees vertically) from the center of the optic disc (Rohrschneider, 2004). For a summary of participant information, see Table 1.

Fixation stability in the eye tracker

Participants first completed a fixation stability task in the eye tracker with three viewing conditions: monocular left, monocular right, and binocular. Individuals were instructed to look at a fixation cross (the same as in the scotoma mapping task, see below) for 10 seconds without blinking, while the eye position was recorded. The start and end of the 10 second presentation were signaled by a brief auditory tone (100 ms, 500 Hz). The distribution of fixations was fit with a bivariate contour ellipse. We used the long axis of the ellipse that fit 99% of the saccades as the radius of the acceptance region for fixation during the mapping procedure. If participants had difficulty keeping their eyes in that window, we used a fixed acceptance region of 3 degrees radius for fixation.

Scotoma mapping in the eye tracker

To determine the extent and location of the binocular scotoma in the B group and of the monocular scotoma or optic disc in the M and C groups, we mapped their

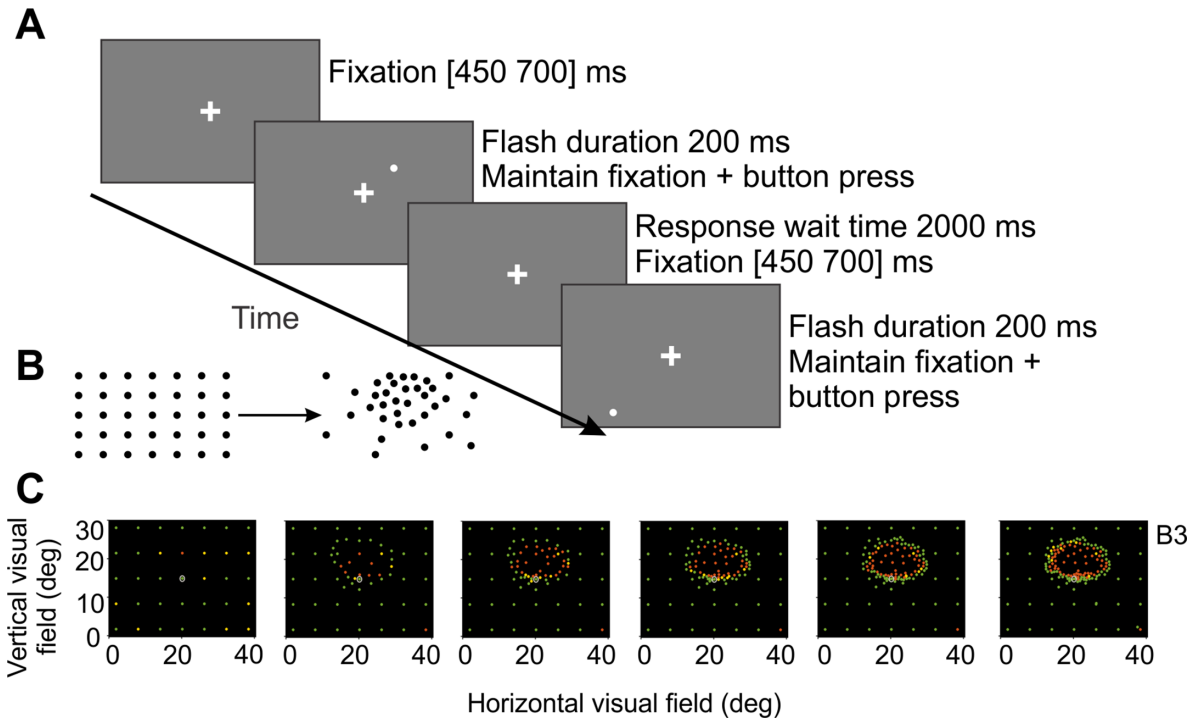

Figure 1. (A) Time course of scotoma mapping procedure. (B) Illustration of coarse-to-fine grids. (C) Steps in probing the visual field for one participant with central fixation. One panel represents one session and the dots are cumulative. A green dot represents a probed region seen twice. A red dot is a region missed twice. A yellow dot is when the participant had seen it once and missed it once. The white circle represents the position of the PRL for MD participants or fovea for control participants, at the screen center.

visual field. We also mapped the monocular scotomata for one participant in the B group, who had stable fixation under monocular viewing with both eyes. Each session consisted of 70 trials. On average, M and C participants completed two sessions for the binocular viewing condition and four sessions for each monocular viewing condition. The B participants did on average five sessions for each of the viewing conditions. The sessions for one viewing condition were typically conducted on the same day, separated by 5-minute breaks. Each session could last from 3 to 15 minutes depending on participants' fixation stability. On average, a monocular session lasted 4.66 minutes (SD = 1.81) for participants with MD and 5.56 minutes (SD = 1.97) for controls, whereas a binocular session lasted 7.03 minutes (SD = 3.57) for participants with MD and 3.8 minutes (SD = 0.84) for controls. Binocular scotoma mapping for B participants is the critical condition in this paper and the total time for these mapping sessions was 26 minutes (B2), 33 minutes (B4), 31 minutes (B3), 1 hour and 23 minutes (B1), 36 minutes (B5), and 24 minutes (B6). B1 and B6 had very large scotomata; B1 was willing to let us probe the scotoma boundary extensively.

At the beginning of each trial, participants looked at the fixation cross for a period varying between 450 and 700 ms (sampled from a uniform distribution) and were instructed to maintain fixation throughout the trial (Figure 1A). Gaze was restricted to a central tolerance window according to the individual fixation stability criterion (on average, 2.89 degrees [SD = 0.8] in radius, see above); the trial would not start if gaze wandered outside the fixation window. If gaze was maintained within the fixation window during the fixation period, a dot was briefly flashed on screen for 200 ms and participants had to press a button within 2 seconds if they detected it. If the participant made a saccade or blinked during stimulus duration, the trial was discarded and that probe location was retested at the end of the session. If the participant pressed the button, there was a post-response time period varying between 0 and 1000 ms (sampled from a uniform distribution) before the next trial, so that the probe onset time was not predictable. There was no additional intertrial interval and the fixation cross was always displayed on the screen, such that participants had no external cue of trial start. If the participant pressed the response button during this intertrial interval or within 325 ms of the start of probe presentation (minimum manual response time for this age group as estimated by Der & Deary, 2006; Nebes, 1978), we counted the response as a false alarm, as this was not likely to be a target-activated response. In each session, we probed 35 locations twice, according to a

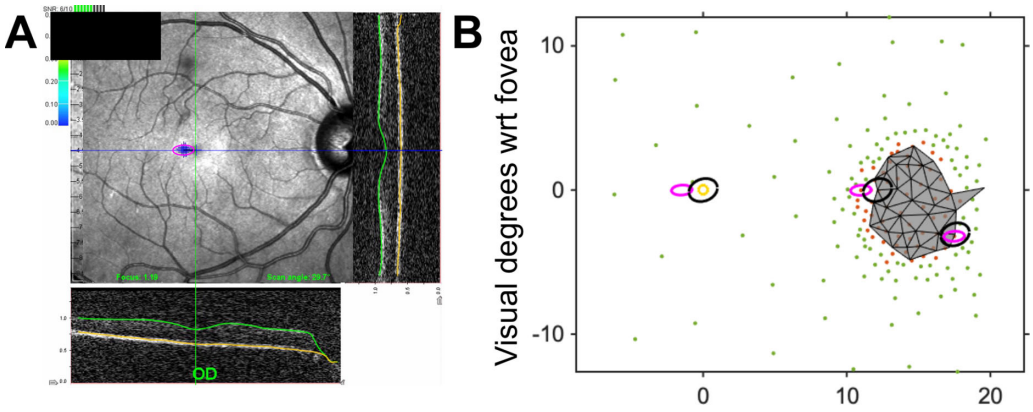

Figure 2. (A) Fundus image of the right eye for a control participant (C4) in the Optos OCT/SLO. The intersection of the green and blue lines represents the foveal pit, obtained through a cross-sectional topography map. This location is represented by a yellow open circle in panel B. The blue crosses represent the fixation loci over a 10 second period with the pink ellipse indicating the BCEA. This fundus image illustrates the observed offset between the anatomical position of the foveal pit and the fixation locus (pink ellipse) for controls in our Optos OCT/SLO. (B) Illustration of the methods used to compute the *d'* value between the monocular optic disc maps obtained in the eye tracker (depicted as the gray region) and SLO microperimetry (unseen and seen flash locations depicted by red and green dots), for the same control participant. The yellow open circle marks the location of the foveal pit; the black ellipse (displayed centered on the foveal pit and around the scotoma boundary) represents the BCEA of fixation stability during probe presentation in the eye tracker. The pink ellipse represents the BCEA of fixation stability measured in the SLO, and is plotted at the same relative location to the foveal pit as shown in A, as well as around two unseen SLO flashes. The overlapping black and pink ellipses illustrate two instances of the method used to determine if an SLO point at the edge of the eye tracker map was within the combined fixation error of the SLO and the eye tracker.

custom coarse-to-fine grid design (Figure 1B). For the first session, the flashed dots were displayed on a 7 × 5 grid that spanned a 36.4 × 26.3 degrees area. The presentation order for each dot location was randomly chosen and repeated twice. Misses were counted and if a location was missed on one or both presentations, it was considered a potential scotoma location. To probe this and neighboring locations at a finer scale in the following sessions, we manually chose test locations. To select the 35 new probe locations, we first plotted the visual field with all the tested probed locations. Out of the 35 points, 10 were allocated to retest partially seen (i.e. missed once and seen once) and seen (i.e. seen on both repetitions) locations, and the remaining 25 points were used to further probe the shape and edges of the scotoma (Figure 1C). The number of fine grid sessions was contingent on both scotoma characteristics (size, shape, and compactness) and participant fatigue.

Comparing monocular maps in the SLO/OCT and the eye tracker

To quantitatively assess how the monocular maps of the optic disc in the eye tracker matched the microperimetry of the optic disc in the SLO, we determined the agreement between unseen points in the two maps. First, we overlaid the monocular maps by aligning the fixation loci for eye tracker and SLO. Because we noticed an offset in our Optos SLO/OCT between the anatomic position of the foveal pit and the fixation locus in controls (Figure 2A), we corrected the individual offset when it was greater than the distribution of natural fixation offsets from the fovea (unpublished data provided to us by W. H. Seiple, distribution with a horizontal standard deviation of 0.77 and vertical standard deviation of 0.84). This correction was applied for five eyes out of the nine in participants with a spared fovea. Second, we calculated a *d'* value from the hits and false alarms to represent the agreement between the optic disc maps in the SLO and the eye tracker maps. If an unseen (red) point in the SLO map fell within the optic disc boundary in the eye tracker map, it was counted as a hit; if it fell well outside the eye tracker map, it was counted as a false alarm. We also took into account fixation instability in the SLO and eye tracker (see Figure 2B), especially because locations of unseen and seen flashes in the SLO were probed only once. For points on the edges of the SLO and eye tracker maps we plotted the BCEA of fixation stability measured in each of these devices. Any point in the SLO map that was within the sum of fixation instability estimated in the SLO and the eye tracker was excluded (i.e. it did not count as either a hit or a false alarm). Figure 2B illustrates two instances of unseen points in the SLO that fell outside the optic disc boundary estimated in the eye tracker but were not counted as false alarms because they were within the combined fixation instability. To the right of the

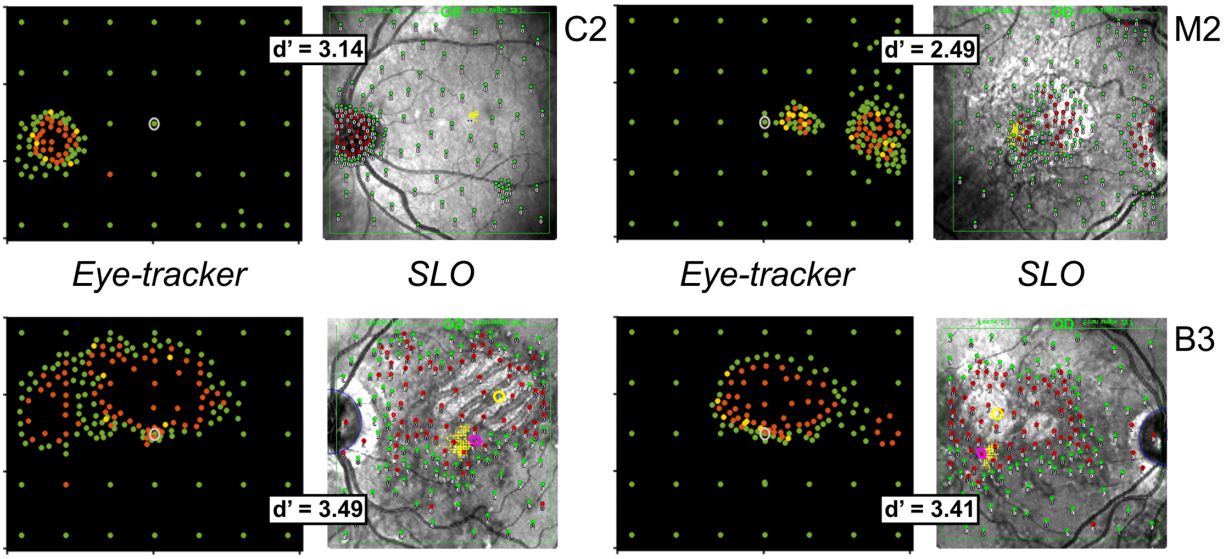

Figure 3. Comparison between the monocular scotoma maps from the eye tracker and SLO microperimetry in one eye of a control participant (C2, first row, left), the affected eye of a participant with a monocular scotoma (M2, first row, right) and both eyes of a participant with binocular MD (B3, second row). The *d'* value for each comparison is shown in the boxed text. For each comparison, the eye-tracker maps are on the left and the SLO maps on the right. For the eye tracker map, see legend Figure 1C. For the SLO monocular microperimetry, the red and green dots represent the locations of unseen and seen flashes. The small yellow crosses represent the fixation loci during perimetry. The pink ellipse represents the BCEA during the 10 seconds fixation stability assessment. The yellow open circle marks the location of the foveal pit, obtained through a cross-sectional topography map obtained using the OCT. Note: the SLO images have been flipped vertically to be consistent with the eye-tracker map measured in visual field coordinates.

gray area representing the optic disc estimate from the eye tracker, is an unseen point in the SLO surrounded by a pink ellipse representing fixation instability in the SLO. The black ellipse represents the fixation instability of the nearest location on the optic disc boundary estimated from the eye tracker. In this case, the black ellipse overlaps completely with the pink ellipse. To the left of the gray area, the pink and black ellipses also overlap, although partially. Both cases represent instances for which a point in the SLO was within the sum of fixation errors of the two measurement methods.

Results

Monocular scotoma mapping

To evaluate whether the eye tracker can serve as a sensitive tool to demarcate the binocular scotoma, we first mapped monocular scotomata in order to directly compare them to those obtained in the SLO (Figure 3). As proof of concept, we first mapped the optic disc in each eye for controls (see Figure 3, first panel). Green, yellow, and red dots represent a probed region seen twice, once, and not seen, respectively, across the two presentations at each location. To estimate the optic disc center, we used the center of mass of the BCEA of the missed dots. The eye tracker estimates of the horizontal and vertical distance between the optic disc and fovea were on average 14.36 degrees (SD = 0.60) and −1.61 degrees (SD = 0.65) across eyes for the four control participants, which are within the previously reported distance between the optic nerve head and the fovea in healthy eyes (i.e. 15.5 ± 1.1 degrees [13.0 to 17.9 degrees] horizontally and −1.5 ± 0.9 degrees [−3.65 to 0.65 degrees] vertically; Rohrschneider, 2004). To quantitively assess how the monocular maps of the optic disc in the eye tracker matched the microperimetry of the optic disc in the SLO, we determined the agreement between unseen red points in the two maps after having aligned the fixation loci for eye tracker and SLO. The average *d'* value calculated from the hits and false alarms was 2.78 (SD = 1.36) across controls, demonstrating excellent agreement between the monocular maps of the optic disc in the eye tracker and the SLO (the eye tracker and SLO maps for the left eye of a control observer are compared in the top left panel of Figure 3). Having established this correspondence for controls, we mapped monocular scotomata in two patients with AMD (participants M2 and M3) and a patient with Stargardt's disease (participant B3), who demonstrated sufficient fixation stability in each eye to enable monocular mapping of both eyes (the data for the eye with monocular scotoma

for M2 and both eyes for the binocular scotoma participant B3 are shown in the upper right and lower panels of Figure 3, respectively). For all affected MD eyes, the monocular scotoma map from the eye tracker includes the optic disc. As was the case for control participants, the similarity between monocular maps in the eye tracker and SLO was consistent with respect to size and shape (*d'* value = 2.31 [SD = 1.2], on average). Thus, the eye tracker appeared to be an adequate tool to map the optic discs for controls and the monocular scotomata for participants with MD, validating its use to map the binocular scotoma.

Binocular scotoma mapping

Figure 1C illustrates the manual coarse-to-fine grid when probing the binocular visual field for participant B3. Each session is represented in one panel; the dots are plotted cumulatively in each panel. Across sessions, the mapping of the binocular scotoma improves, and within a few sessions, we observe a precise map of binocular field loss for this participant. Figure 4 represents the binocular scotoma of all B participants with respect to their fixation stability, represented by a kernel density plot of fixation distribution (Crossland, Sims, Galbraith, & Rubin, 2004; see Figure 5). The bounding area for the binocular scotoma is estimated by a polygon that envelops the set of missed points (using MATLAB's alphaShape function) with a scotoma area of 3.73, 26.43, 108.69, 281.99, 159.43, and 430.40 degrees^2 for participants B2, B4, B3, B1, B5, and B6, respectively. We calculated the rate of false alarms in the binocular scotoma map by considering any button press with a latency shorter than 325 ms following target onset (based on manual reaction times for elderly people in simple detection tasks; Der & Deary, 2006; Nebes, 1978), as well as any that occurred in the intertrial interval. On average, the rate of false alarms was 1.87% (SD = 1.57) of total trials, indicating that participants very rarely responded before seeing the flash. Alongside the binocular scotoma maps for each participant in Figure 4 are the monocular SLO perimetry maps for the left and right eyes, respectively. For participants B5 and B6, fixation in one or both eyes was not stable enough to do SLO microperimetry, so the panels show just the retinal image with the fixation locus superimposed. Aligning the monocular SLO maps on the respective fovea of each eye (yellow circle) provides an estimate of the overlap of the two eyes' scotomata. Importantly, the binocular scotoma estimate for all participants with bilateral field loss is consistent with this overlap region, no matter whether the two eyes' scotomata overlap minimally (B2 and B3) or substantially (B1, B4, B5, and B6). Therefore, our method for binocular scotoma mapping was highly effective for a large range of sizes and shapes of binocular scotoma from small (B2 and B4) to extensive (B1, B5, and B6). It is also noteworthy that the eye tracker enabled us to map the binocular scotoma for two participants whose monocular scotoma, in at least one eye, could not be estimated with the SLO. Indeed, for B5, we could only get the monocular map for the right eye and for B6, we could not locate intact retinal locations in the SLO. Unsurprisingly, individuals with a monocular scotoma and control participants had no measurable binocular scotoma under conditions of binocular viewing.

Fixation stability

The fidelity of the binocular scotoma estimated from the eye tracker depends crucially on how stable the participants' eyes were while maintaining fixation during stimuli presentation. Figure 5 represents the kernel density plot of fixation distribution (Crossland et al., 2004) during the 200 ms probe presentation, for all trials. We observed that half of the participants used a single (foveal or peripheral) fixation locus during the fixation interval (participants B2, B4, B6, M1, M2, C2, and C4), and the other half used two or more fixation loci, which were tightly clustered (participants B1, B3, B5, M3, C1, and C3). Figure 5 plots representative participants who demonstrated single or multiple clustered fixation loci from each of the M, C, and B groups. Note, the scale for Figure 5 is zoomed in compared to Figure 4. We considered both the horizontal and vertical spread of kernel density estimate of fixation distribution and took the larger value to characterize the fixation dispersion. Participants with binocular scotoma had less stable fixation during the mapping procedure (dispersion of 3.45 degrees [SD = 1.52], on average) than participants with monocular scotoma (dispersion of 2 degrees [SD = 0.74], on average) and control participants (dispersion of 1.29 degrees [SD = 0.43], on average).

Discussion

Determining the precise location and extent of the binocular scotoma is important for the rehabilitation of residual vision in central field loss. Here, we show that a coarse-to-fine mapping strategy, where locations are selected recursively to map the extent and boundaries of the scotoma while fixation is monitored, can provide an accurate representation of the binocular scotoma. Both the estimation of the binocular scotoma and the adaptive testing are aspects that are different from standard automated perimetry methods. For instance, automated perimetry in the Humphrey Field Analyzer is monocular and uses a fixed spacing of

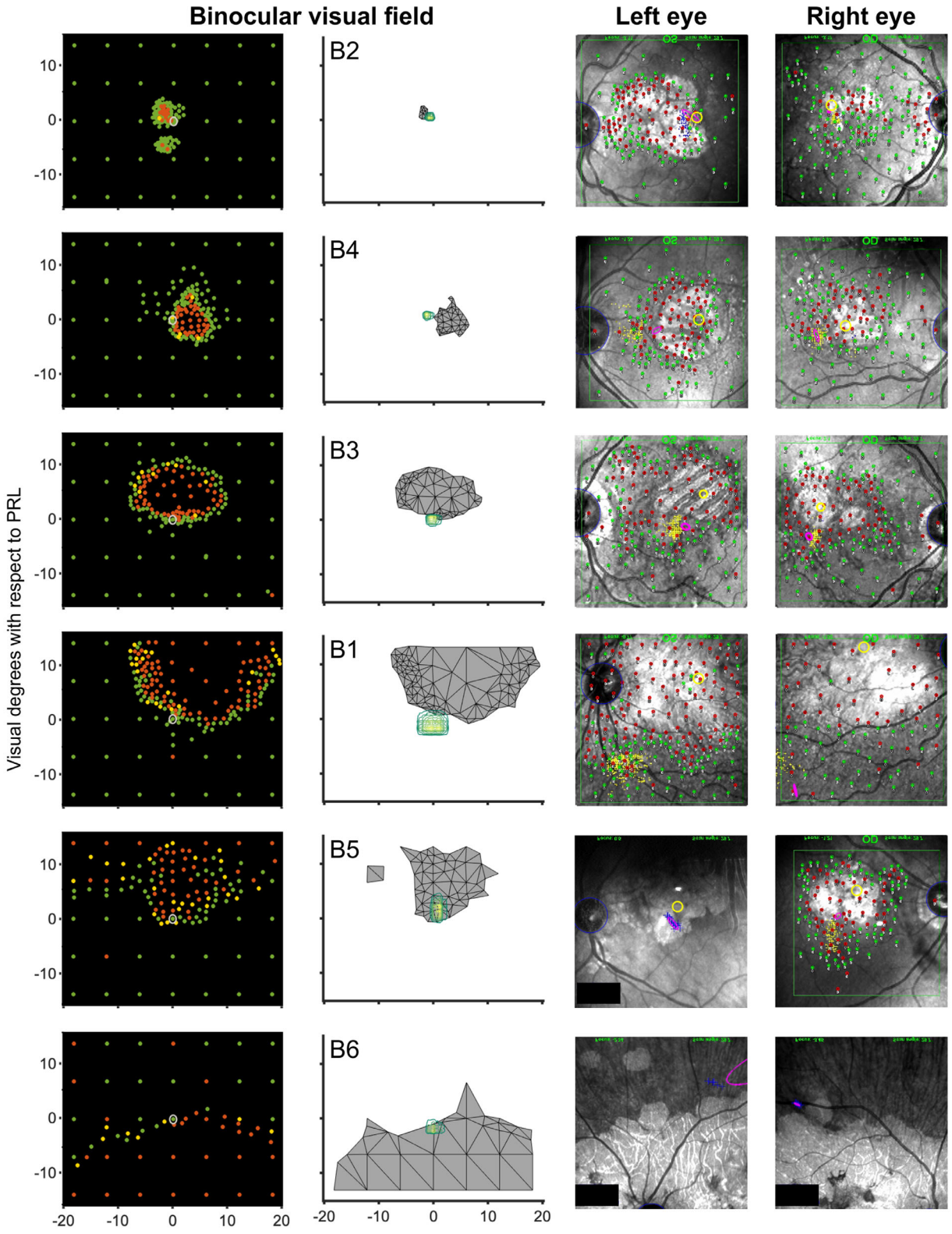

Figure 4. First and second columns: Eye tracker map of binocular scotoma of all participants with binocular MD (see legend Figure 1C), estimated as a polygon that envelops the set of missed points, with respect to their PRL. Their fixation stability is represented by a kernel density plot of fixation distribution. Third and fourth columns: SLO microperimetry for the left and right eyes (see legend Figure 3). When fixation stability was too poor to conduct microperimetry, the retinal image during the fixation test is provided (for participants B5 and B6, the retinal damage around the PRL is visible). Note: the SLO images have been flipped vertically to be consistent with the eye-tracker map measured in visual field coordinates.

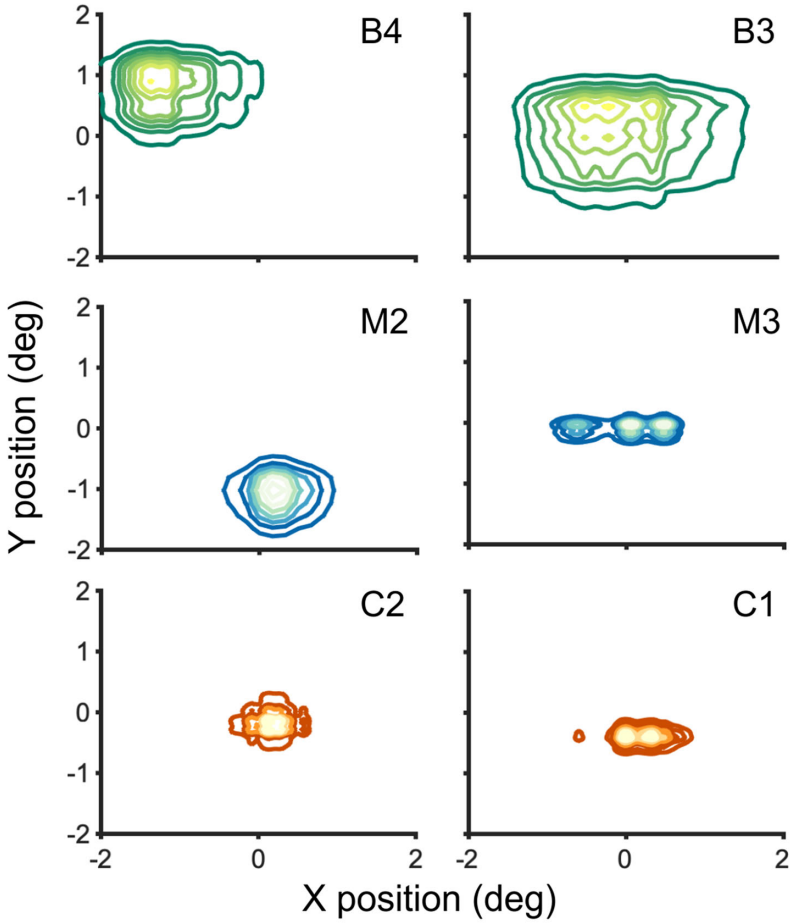

Figure 5. Different patterns of fixation stability across the three groups of participants (binocular scotoma in green, monocular scotoma in blue, and control in red). Fixation stability is represented by a kernel density plot of fixation distribution. The left and right columns show a representative participant from each group that has a single PRL and more than one PRL, respectively. Note the zoomed-in scale compared to Figure 4.

6 degrees between probe locations, rendering the mapping too crude to provide fine details about the scotoma boundary. Other methods, such as manual microperimetry in the SLO or spectral-domain OCT, can map the region of the retinal lesion in detail (e.g. Acton, Smith, Hood, & Greenstein, 2012), but have the drawback of being monocular. The one exception to this is the high-resolution custom binocular SLO (Chung et al., 2020), which is limited to a visual field of 10 degrees.

A precise map of the binocular scotoma is relevant to understanding residual functional vision in MD. It can be useful when one tries to assess performance with respect to vision loss, such as performance accuracy and eye movements characteristics in visual search or a reaching task (e.g. Sullivan & Walker, 2015; Van der Stigchel et al., 2013), or to train an eye-movement strategy with respect to scotoma location to uncover hidden objects of interest (Janssen & Verghese, 2016). Eye-tracker-based perimetry offers a good alternative to map the visual field in detail, even in the absence of fundus-tracking. For instance, Naber, Roelofzen, Fracasso, Bergsma, van Genderen, Porro, and Dumoulin (2018) conducted monocular flicker pupil perimetry using a gaze-contingent stimulus presentation in patients with cerebral visual impairment or glaucoma and obtained similar results as standard monocular automated perimetry. Our study is not the first to attempt to map the binocular scotoma with an eye tracker in MD. Van der Stigchel et al. (2013) measured the detection of a target (1.5 degrees) in 33 locations across a large area (37 × 28 degrees) at a viewing distance of 57 cm. Participants were instructed to maintain fixation at the center of the screen, but it is not clear that eye position was monitored. Sullivan and Walker (2015) mapped the absolute binocular scotoma on a grid of 17 × 12 points spaced 1.7 degrees apart, at a viewing distance of 40 cm. Interestingly, participants were instructed to center their fovea on the screen with the help of a large wagon-wheel stimulus. The head was restrained and eye position was monitored. Bright dots were briefly flashed once at a subset of

135 probe locations chosen randomly. This method had the advantage of probing a large visual field but the random choice of locations could have led to missing critical parts of the scotoma. In addition, it is not clear how well this fovea-centered viewing strategy corresponds to viewing with a PRL. Janssen and Verghese (2016) used a rapid but coarse assessment of the binocular scotoma at viewing distance of 0.9 m, while the PRL was pointing at the screen center. In discrete trials, participants had to fixate a marker and expressly report whether or not they had seen a briefly flashed stimulus. Square targets at two scales (5 and 2.5 degrees) spanned a central region of 25 × 15 degrees or 17.5 × 12.5 degrees, respectively. Each grid location was tested twice, increasing the reliability of the visibility estimate. This method was quick but it lacked the flexibility to probe the binocular scotoma in detail. Importantly, while they measured fixation at the start of the trial, they did not constrain fixation to be at the screen center during the 200 ms target presentation. Shanidze and Verghese (2019) used another type of coarse-to-fine grid at 1 m, while the eye position was monitored. First, they measured the visibility of briefly flashed dots presented on a 5 × 5 grid (17 × 7 degrees) around fixation. Then, another 5 × 5 grid at half the spacing was used to probe any quadrant with missed points. This introduced a certain degree of customization to the individual's scotoma. However, because of the preset scale and spacing, the probed locations did not always provide a detailed profile of the binocular scotoma. Our method combines the strengths of these previous methods by first probing coarsely a region of 36 × 26 degrees and then selecting points manually to refine the edges of the scotoma, while the eye position is constrained to be within a tolerance region around the fixation mark. This iterative process divides the visual field assessment into shorter sessions, and provides the flexibility to decide how extensively to probe the binocular scotoma given the participant's fatigue. Finally, each location is tested twice within sessions and the manual selection in the fine grid offers a retest between sessions of some locations for validity.

Our binocular scotoma mapping procedure was used under static viewing conditions at a single viewing distance (1 m). Thus, it ignores the potential change in alignment of the eyes during pursuit in 2 or 3 dimensions (depth). Arditi (1988) has shown previously that the binocular scotoma is a 3-dimensional volume that depends on vergence angle. Our estimate of the static scotoma is similar to previous methods of mapping the binocular scotoma with an eye tracker (e.g. Janssen & Verghese, 2016; Sullivan & Walker, 2015), although it has the advantage that it provides the flexibility to map scotoma extent more precisely. However, in the event that the volume scotoma is needed, our eye-tracker-based method could be used to map the binocular scotoma mapping at several depths from the fixation plane (see also Tarita-Nistor et al., 2015), unlike the SLO. Although eye-tracker-based methods are an improvement over the California Central Visual Field test (Mattingly Low Vision, Inc.), which does not monitor fixation, they are still limited by variations in fixation or switching between multiple PRLs during mapping that can cause errors in the binocular scotoma map. However, the careful documentation of eye-position in our participants showed that fixation remained stable during probe presentation. The eye-tracker-based estimate of the binocular scotoma also has the advantage of making no assumptions about binocular alignment, as in the Ghahghaei and Walker (2016) algorithm, which aligns the two monocular scotoma maps by superimposing the respective foveae of the two eyes to estimate the binocular scotoma. Finally, our method of measuring the binocular scotoma has the crucial advantage that it does not depend on monocular maps from the two eyes. It works even when fixation in the weaker eye is so poor that the scotoma cannot be mapped in the SLO. Thus, we believe that our binocular scotoma mapping method provides a precise estimate of the location and extent of the functional scotoma that is relevant to vision in everyday life.

Keywords: macular degeneration, binocular scotoma, eye-tracker mapping, residual vision

Acknowledgments

The authors thank Saeideh Ghahghaei for providing the script of the algorithm from Ghahghaei and Walker (2016), William Seiple for discussions of microperimetry in the Optos SLO, Natela Shanidze for comments on a previous version of the manuscript, and Don Fletcher for referring the patients who participated in this study.

Supported by a Fulbright grant (C.V.), a Rachel C. Atkinson & C.V. Starr postdoctoral fellowship (C.V.) and a NIH grant NIH R01 EY029730 (P.V.).

Commercial relationships: none.
Corresponding author: Cécile Vullings.
Email: cecile.vullings@gmail.com.
Address: 2318 Fillmore Street, San Francisco, CA 94115, USA.

References

Acton, J. H., Smith, T. R., Hood, D. C., & Greenstein, V. C. (2012). Relationship between retinal

layer thickness and the visual field in early age-related macular degeneration. *Investigative Ophthalmology and Visual Science, 53*(12), 7618–7624, https://doi.org/10.1167/iovs.12-10361.

Arditi, A. (1988). The volume visual field: A basis for functional perimetry. *Clinical Vision Sciences, 3*(3), 173–183.

Aspinall, P. A., Borooah, S., Al Alouch, C., Roe, J., Laude, A., & Gupta, R. et al. (2014). Gaze and pupil changes during navigation in age-related macular degeneration. *British Journal of Ophthalmology*, *98*(10), 1393–1397.

Bernard, J.-B., & Chung, S. T. L. (2016). The role of external features in face recognition with central vision loss: A pilot study. *Optometry and Vision Science*, *93*(5), 510–520.

Brainard, D. H. (1997). The Psychophysics Toolbox. *Spatial Vision, 10*, 433–436.

Brandao, L. M., Ledolter, A. A., Schötzau, A., & Palmowski-Wolfe, A. M. (2016). Comparison of two different OCT systems: Retina layer segmentation and impact on structure-function analysis in glaucoma. *Journal of Ophthalmology, 2016*, 1–9.

Chung, S. T. L. (2020). Reading in the presence of macular disease: a mini-review. *Ophthalmic and Physiological Optics*, *40*(2), 171–186.

Chung, S. T., Li, R. W., Ağaoğlu, M. N., Tiruveedhula, P. K., & Roorda, A. (2020). Binocular properties of fixational eye movements as assessed using a high-resolution binocular scanning laser ophthalmoscope. *Investigative Ophthalmology & Visual Science, 61*(7), 1708–1708.

Cohen, S. Y., Lamarque, F., Saucet, J.-C., Provent, P., Langram, C., & LeGargasson, J.-F. (2003). Filling-in phenomenon in patients with age-related macular degeneration: Differences regarding uni- or bilaterality of central scotoma. *Graefe's Archive for Clinical and Experimental Ophthalmology, 241*(10), 785–791, https://doi.org/10.1007/s00417-003-0744-3.

Crossland, M. D., Sims, M., Galbraith, R. F., & Rubin, G. S. (2004). Evaluation of a new quantitative technique to assess the number and extent of preferred retinal loci in macular disease. *Vision Research, 44*(13), 1537–1546.

Der, G., & Deary, I. J. (2006). Age and sex differences in reaction time in adulthood: Results from the United Kingdom health and lifestyle survey. *Psychology and Aging, 21*(1), 62–73.

Ellingham, R. B., Waldock, A., & Harrad, R. A. (1993). Visual disturbance of the uncovered eye in patients wearing an eye patch. *Eye, 7*(6), 775–778.

Fletcher, D. C., Schuchard, R. A., & Renninger, L. W. (2012). Patient awareness of binocular central scotoma in age-related macular degeneration. *Optometry and Vision Science, 89*(9), 1395–1398.

Ghahghaei, S., & Walker, L. (2016). SKERI-Optos: A graphical user interface to map scotoma and PRL with the Optos OCT/SLO. *Journal of Vision, 16*(4), 40–41.

Janssen, C. P., & Verghese, P. (2016). Training eye movements for visual search in individuals with macular degeneration. *Journal of Vision, 16*(15), 1–20.

Kabanarou, S. A., Crossland, M. D., Bellmann, C., Rees, A., Culham, L. E., & Rubin, G. S. (2006). Gaze changes with binocular versus monocular viewing in age-related macular degeneration. *Ophthalmology*, *113*(12), 2251–2258.

Naber, M., Roelofzen, C., Fracasso, A., Bergsma, D. P., van Genderen, M., Porro, G. L., . . . Dumoulin, S. O. (2018). Gaze-contingent flicker pupil perimetry detects scotomas in patients with cerebral visual impairments or glaucoma. *Frontiers in Neurology, 9*, 1–12.

Nebes, R. D. (1978). Vocal versus manual response as a determinant of age difference in simple reaction time. *Journals of Gerontology, 33*(6), 884–889.

Nilforushan, N., Nassiri, N., Moghimi, S., Law, S. K., Giaconi, J. A., & Coleman, A. L., et al. (2012). Structure-function relationships between spectral-domain OCT and standard achromatic perimetry. *Investigative Ophthalmology and Visual Science, 53*(6), 2740–2748.

Pelli, D. G. (1997). The VideoToolbox software for visual psychophysics: transforming numbers into movies. *Spatial Vision, 10*, 437–442.

Pfau, M., Müller, P. L., Von der Emde, L., Lindner, M., Möller, P. T., & Fleckenstein, M. et al. (2020). Mesopic and dark-adapted two-color fundus-controlled perimetry in geographic atrophy secondary to age-related macular degeneration. *Retina, 40*, 169–180.

Rohrschneider, K. (2004). Determination of the location of the fovea on the fundus. *Investigative Ophthalmology & Visual Science, 45*(9), 3257–3258.

Safran, A. B., & Landis, T. (1999). From cortical plasticity to unawareness of visual field defects. *Journal of Neuro-Ophthalmology: The Official Journal of the North American Neuro-Ophthalmology Society*, *19*(2), 84–88.

Shanidze, N., & Verghese, P. (2019). Motion perception in central field loss. *Journal of Vision, 19*(14), 1–20.

Steinman, R. M. (1965). Effect of target size, luminance, and color on monocular fixation. *Journal of the Optical Society of America, 55*, 1158–1165.

Sullivan, B., & Walker, L. (2015). Comparing the fixational and functional preferred retinal location in a pointing task. *Vision Research, 116*, 68–79.

Tarita-Nistor, L., Eizenman, M., Landon-Brace, N., Markowitz, S. N., Steinbach, M. J., & González, E.G., (2015). Identifying the absolute locations of the PRLs during binocular viewing. *Optometry and Vision Science, 92*, 863–872.

Timberlake, G. T., Mainster, M. A., Webb, R. H., Hughes, G. W., & Trempe, C. L. (1982). Retinal localization of scotomata by scanning laser ophthalmoscopy. *Investigative Ophthalmology and Visual Science, 22*, 91–97.

Urata, C. N., Mariottoni, E. B., Jammal, A. A., Ogata, N. G., Thompson, A. C., & Berchuck, S. I., et al. (2020). Comparison of short- and long-term variability in standard perimetry and spectral domain optical coherence tomography in glaucoma. *American Journal of Ophthalmology, 210*, 19–25, https://doi.org/10.1016/j.ajo.2019.10.034.

Van der Stigchel, S., Bethlehem, R. A. I., Klein, B. P., Berendschot, T. T. J. M., Nijboer, T. C. W., & Dumoulin, S. O. (2013). Macular degeneration affects eye movement behavior during visual search. *Frontiers in Psychology*, *4*, 1–9.

Verghese, P., Tyson, T. L., Ghahghaei, S., & Fletcher, D. C. (2016). Depth perception and grasp in central field loss. *Investigative Ophthalmology and Visual Science*, *57*(3), 1476–1487.

Von Noorden, G. K., & Mackensen, G. (1962). Phenomenology of eccentric fixation. *American Journal of Ophthalmology, 53*, 642–661.

Wiecek, E. K., Jackson, M. L., & Bex, P. J. (2015). Binocular microperimetry with simulated asymmetric bilateral scotomas. *Investigative Ophthalmology & Visual Science, 56*(7), 549–549.

Zur, D., & Ullman, S. (2003). Filling-in of retinal scotomas. *Vision Research, 43*, 971–982.